# Mass-to-light ratios for Elliptical galaxies

Derek Land

Supervisor: Professor R.H. Sanders

January 28, 2008
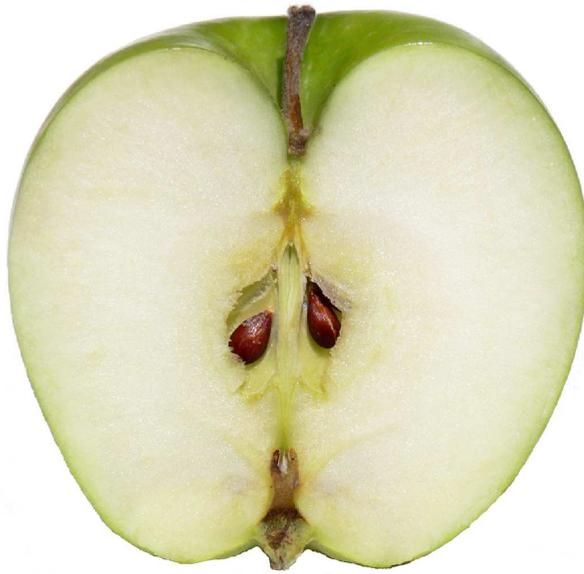
Abstract

With Newtonian dynamics, the masses of elliptical galaxies do not explain the masses derived from the luminosity of the galaxy itself. In this research, different methods to determine the masses of galaxies are compared to mass estimates of the same objects with modified Newtonian dynamics.

We conclude that the modified Newtonian dynamics mass estimates agree well with stellar population models and mass estimates using lensing data. A problem for X-ray mass measurements is the assumption of hydrostatic equilibrium. This assumption might not be valid, which might explain the sometimes extremely high mass-to-light ratios for these objects.

Contents

1 Introduction

In 1937 Fritz Zwicky published a paper (Zwicky, 1937) in which he applied the Virial Theorem in order to calculate the dynamical mass of the Coma Cluster. After comparing the dynamical mass and the luminosity of the cluster he astonishingly found that the mass inferred from the luminosity of the cluster was about 400 times less then its dynamical mass. The gravitational attraction of the visible mass could not explain the line of sight velocities of the cluster. To explain the differences between the dynamical mass and the luminosity, he concluded that there must be some kind of non-visible form of matter, i.e. 'dark matter'.

In the 1970s, sensitive spectrographs made it possible to measure the velocity curve of edge-on spiral galaxies. Rogstad and Shostak (1972) showed that flat rotation curves exist up to 50kpc from the core of luminous spiral galaxies. The difference between the luminous mass and virial mass observed in spiral galaxies turned out to be part of a bigger missing mass problem. From dwarf spheroidal galaxies up to super clusters of galaxies, all pressure supported systems seem to be missing mass.

1.1 Goal

It is well known that spiral galaxies have a missing mass problem, for elliptical galaxies the situation is less clear. In order to quantify and identify the missing mass problem, the mass of elliptical galaxies needs to be measured. In this report three different methods will be used: modelling of stellar kinematics, gravitational lenses and hot gas in order to estimate the mass, and thus the missing mass of a galaxy.

In section 3 the modelling of stellar kinematics is used to determine mass-to-light ratios for a set of 25 elliptical galaxies from their observed velocity dispersion and effective radius. In section 4 data from the Sloan Lens ACS Survey is applied to the fundamental plane theorem to obtain mass estimates without the dependency on the luminous matter. And in section 5 X-ray emitting gas observed by the Chandra and XMM-Newton X-ray satellite observatories are used to construct the total mass of a galaxy from the hot gas distribution.

In section 6 the results from the three different mass estimates are combined and compared to other estimates, in order to attempt to answer the question: can Modified Newtonian Dynamics explain the missing mass problem without dark matter in elliptical galaxies?

2 Background

2.1 Dark Matter

With Newtonian dynamics, extra mass is required to explain the observed differences between the dynamical mass and the luminosity of (clusters of) galaxies. The only possibilities explaining the missing mass problem are unknown particles which do not or only weakly interact with baryonic matter, or theories which deviate from the known theory of gravity.

2.1.1 Baryonic dark matter

Baryonic dark matter is ordinary matter, like protons and neutrons, except baryonic dark matter does not emit electromagnetic radiation. It is not clear why baryonic dark matter does not emit electromagnetic radiation. There are different possibilities in what kind of form dark matter can exist. A limited review is given below:

The Initial Mass Function (IMF) is our estimate of the number of objects formed with a certain mass. Often the Salpeter IMF (Salpeter, 1955) is used, this is a power law

$$\frac{dn}{d\ln m} \approx m^{-x} \tag{1}$$

where n is the number density of objects with mass m. For the Salpeter IMF the exponent is $x = 1.35$. Integrating from a certain minimum mass till infinity gives the total mass. But this total mass depends on the minimum mass used in the integration. If for the Salpeter IMF the minimum mass is changed by a factor of 7.2 the total mass is enlarged by a factor of 2, reducing the required amounts of dark matter. Changing the minimum mass of the IMF is constraint by the number of low mass objects which can exist.

Low mass objects have a lower limit below which it is not possible to collapse. This limit is the Jeans mass which depends on the maximum scale, density and temperature for which a perturbation can be stable. If a cloud of gas is less massive then the Jeans mass, the cloud will not collapse.

Forming low mass stars ($M_* \ll M_\odot$ from a single cloud of gas is not possible because the mass of the cloud will stay below the Jeans mass. To be able to create low mass objects, there must be some larger cloud of gas which fragments into smaller pieces. When a cloud collapses the internal energy rises, heating the gas and halting the collapse. The cooling has to be fast; if the cooling is slow and the cloud is pressure dominated the cloud will collapse without forming smaller substructures. In order to explain the missing mass problem with small, collapsed cloud fragments, a lot of these objects need to be around. The process of forming small, Jupiter sized, objects is difficult and not well understood, making it unlikely that all the dark matter can be explained by these objects.

Small bodies such as comets, dust grains or asteroids, which are held together due to molecular forces are an unlikely source of dark matter. Although they are too small and faint to detect at any astronomical distance beyond the solar

system, they can not represent much of the missing mass. They mostly consist of carbon, silicon and oxygen, which are not common compared to hydrogen in the universe. At maximum there could be 1% of the hydrogen mass hidden in these small bodies which is not enough to explain dark matter.

The collection of small and low mass objects are also called MACHOs, Massive Astrophysical Compact Halo Object. Tisserand et al. (2007) ruled out MACHOs in the mass range of $0.6 \times 10^{-7} M_\odot < M < 15 M_\odot$ to be the primary occupants of the Milky Way Halo. They tried to detect the MACHOs by monitoring the change of brightness of many stars in the Magellanic Clouds when a MACHO in the Milky Way Halo moves in front of the background star. Instead of the 39 predicted MACHO events they found only one candidate.

Massive stellar black holes formed during the collapse of massive stars ($M_* \lesssim 100 M_\odot$) pollute their environment by expelling parts of their matter before collapsing into a black hole. The abundance of heavy elements in the expelled matter puts constraints on the number of massive blackholes which can be formed without interfering with the universal mass density. Carr et al. (1984) showed that $\Omega_{BH} \lesssim 10^{-4}$, where Ω_{BH} is the contribution of massive black holes to the universal mass density.

For stars much heavier than $M_* \gtrsim 100 M_\odot$, there is no such constraint since they collapse without polluting their environment (Carr et al., 1984). But there is an upper limit on the mass of the black holes due to the constraints from the velocity dispersion-age relation in the solar neighbourhood. Another constraint is the absence of lensing effects in most quasars, making the cosmological number density of massive black holes formed from massive stars negligible (Canizares, 1982).

2.1.2   Non-baryonic dark matter

Non-baryonic dark matter is matter consisting of non-baryonic particles. Many candidate particles are predicted by extentions to the standard model but only one dark matter candidate has been detected so far.

Neutrinos were postulated by Wolfgang Pauli in 1930 to explain the conservation of energy and momentum in beta decay. In 1995 the Nobel prize was awarded to Frederick Reines for the detection of the free neutrino in experiments carried out in 1956. The neutrino has no charge, half integer spin and comes in three flavours: e-, μ- and τ-neutrino. They are formed by beta decay of three other leptons, the electron, muon and tau lepton respectively. In 1998 experiments have shown that neutrinos possess mass, since it is possible for them to oscillate from one flavour to another.

From Solar neutrinos it is known that they can change shape between being emitted from the Sun and observed at Earth. This oscillating process gives information about the mass differences between the flavours. For the different neutrinos, this mass difference is between $5 \times 10^{-5}\,\text{eV}^2$ and $3 \times 10^{-3}\,\text{eV}^2$. The number density of the different species of neutrinos has been calculated to be $3/11 n_\gamma$ where n_γ is the number density of photons. This results in a few

hundred of neutrinos in every cubic centimetre of the Universe (Ryden, 2003, chapter 8). Combining the numbers for the neutrino density and the missing mass, neutrinos need to have an energy of $4\,\mathrm{eV}$ to explain all the missing mass. Since the three different species have mass differences around $5 \times 10^{-4}\,\mathrm{eV}^2$ this would lead to either three species of neutrinos with almost the same mass, or with a mass $m_\nu \ll 1\,\mathrm{eV}$ meaning there must be another explanation for dark matter.

Neutrinos are considered hot dark matter. They were relativistic when they decoupled from other matter (Weinberg, 1972). Computer simulations on large scale structures in the Universe show that hot matter in the early Universe iron out primordial density fluctuations (Efstathiou and Silk, 1983), making it impossible to grow the small scale structures we observe at the present age of the Universe. The maximum fraction of hot dark matter which would allow the current observed large scale structure in the Universe is about 30 percent, leaving 70 percent for another form of dark matter.

The Axion is another particle which might explain the missing matter. The axion is a pseudo-scalar particle postulated to explain the absence of charge-parity symmetry violation in the strong interaction in quantum chromodynamics. These particles have a small mass and, if they exist, would have formed in the early Universe. The particle is expected to decay into two photons with a life time which exceeds the current age of the Universe for 10 eV axions. When an axion interacts with a magnetic field, it can decay. Experiments trying to detect this axion radiation have so far not resulted in any detection. Axions with a mass above 1 eV are also excluded to be able to explain the missing mass. If such particles would exists, red giant, helium burning stars would emit axions and thus transfer energy. This extra energy needs to be supplied by nuclear fusion and thus reduces their lifetime. The reduction of the lifetime of red giants reduces the number density at any given moment in time, underestimating the observed number density of red giants. Since axions decoupled from matter while being non-relativistic, they are considered cold dark matter, and –contrary to hot dark matter– do not influence the large scale structure growth.

WIMPs or Weakly Interacting Massive Particles are a class of proposed dark matter particles with a mass of a few GeV up to a few hundreds of GeV. In the early Universe they might have been produced by positron-electron annihilation. As long as the temperature of the Universe was above the mass of the WIMP the number density of particles would be comparable to the number density of photons, electrons and positrons. The first proposed WIMP with a mass of around 2 GeV has already been ruled out by the improving sensitivity of the dark matter detectors.

In order to detect WIMPs, there are different signatures which the detectors might detect, for example a yearly modulation of the WIMP flux due to the earths rotation around the sun and an asymmetry in the direction of the WIMPs due to the Sun's motion trough the Milky Way (Spergel, 1988). Other experiments to detect those massive particles so far have set limits on the energy range of the particles. The ZEPLIN and EDELWEISS experiments have set upper limits on the cross section and energy range of the WIMPs. DAMA

claims to have a 6 sigma detection of the recoil of a scattering nucleus but this detection is outside the upper limits provided by ZEPLIN and EDELWEISS (Cooley, 2006).

2.2 Modified Newtonian Dynamics

In 1983 Milgrom proposed an alternative for dark matter by modifying Newtonian dynamics in the low acceleration regime. For Newtonian dynamics to be valid, the mass of a particle must determine the gravitational force, the gravitational force should be universal and Newton's second law is correct.
In Modified Newtonian Dynamics (hereafter MOND) at least one of these condition is no longer valid. In the regime of small accelerations the gravitational force, $F = mg$, where the force F is equal to the mass m times the gravitational acceleration g, is changed into:

$$F = m\frac{g^2}{a_0},\tag{2}$$

with a_0 a new constant with units of acceleration. A heuristic interpolation between the Newtonian regime and MOND is

$$g\mu\left(\frac{g}{a_0}\right) = g_N,\tag{3}$$

where g_N is the Newtonian gravitational acceleration and $\mu(x)$ is the interpolating function: $\mu(x) \approx 1$ when $x \gg 1$ and $\mu(x) \approx x$ when $x \ll 1$. The acceleration constant is the only parameter which has to be constrained by the data. Begeman et al. (1991) used a sample of large galaxies with well-determined rotation curves. Fitting rotation curves to this data with a_0 as a fixed parameter resulted in $a_0 = 1.2 \pm 0.27 \times 10^{-8}\mathrm{cm/s^2}$. This value is remarkably close to the Hubble parameter multiplied by the speed of light (cH_0) which might suggest a connection between MOND and cosmology.

2.3 Newtonian virial theorem

The virial theorem relates the potential energy of a bounded system to the kinetic energy of the sytem. The derivation starts from the scalar moment of inertia I around the origin of a coordinate system, with the point of interest in the origin:

$$I = \sum_k m_k r_k^2,\tag{4}$$

where m_k and r_k are the mass and the position of the k$^{\mathrm{th}}$ particle. Differentiating with respect to time gives:

$$H = \frac{dI}{dt} = 2\sum_k p_k r_k,\tag{5}$$

7

where $p_k = m_k \dot{r}_k$ is the impulse of the particle. Differentiating once more with respect to time gives:

$$
\begin{aligned}
\frac{1}{2}\frac{dH}{dt} &= \sum_k \dot{p}_k r_k + \sum_k p_k \dot{r}_k \\
&= \sum_k F_k r_k + \sum_k m_k v_k^2,
\end{aligned}
\tag{6}
$$

where v_k is the velocity of the kth particle and F_k is the force on the kth particle. For a bound system dH/dt approaches zero relating the kinetic energy to the virial (Clausius, 1870):

$$
\left\langle \sum_k m_k v_k^2 \right\rangle = \left\langle \sum_k F_k r_k \right\rangle.
\tag{7}
$$

For a gravitational bound system, the force can be derived from the potential, U, which results in a virial theorem with the form:

$$
T = -\frac{1}{2}U,
\tag{8}
$$

where T is the kinetic energy of the system.

2.4   Fundamental plane

From the virial theorem several relations can be derived. One of those relates the size of a galaxy R, the surface brightness I and the velocity dispersion σ of elliptical galaxies. For elliptical galaxies the gravitational potential is $U = -GmM/r$ and the kinetic energy is $T = m\sigma^2$. According to the viral theorem (Eq. 8) they are related:

$$
\begin{aligned}
m\sigma^2 &= \frac{GMm}{2R} \\
\sigma^2 &= \frac{G}{2R}L\Upsilon \\
&= \frac{G}{2R}I\Upsilon 2\pi R^2 \\
&= \pi G R I \Upsilon
\end{aligned}
\tag{9}
$$

where $M = \Upsilon L$, with Υ the mass-to-light ratio and the luminosity $L = 2\pi r^2 I$. This relation between the observables I, R and σ^2 is known as the fundamental plane of elliptical galaxies. Besides the mass-to-light ratio which is not well understood, the luminosity and mass profile of the galaxies may not be uniform which gives an extra variable, c, to the fundamental plane:

$$
R = \frac{\sigma^2}{I}\frac{c}{\pi G \Upsilon}.
\tag{10}
$$

8

In 1987, both Dressler et al. and Djorgovski and Davis discovered a linear relation in logarithmic space between the effective radius r_e, the velocity dispersion within this effective radius σ and the projected luminosity density within the effective radius I_e. Djorgovski and Davis (1987) found in the r_G passband:

$$\log a_e = 1.39 \log \sigma - 0.90 \log I_e + \text{constant}, \tag{11}$$

where a_e is related to r_e according to $r_e = a_e \sqrt{1-\epsilon}$ with ϵ the ellipticity of the galaxy. At the same time Dressler et al. (1987) found in the Johnson B passband:

$$\log r_e = 1.325 \log \sigma - 0.825 \log I_e + \text{constant}. \tag{12}$$

More recent observations by Bernardi et al. (2003) in all the Sloan pass-bands found a fundamental plane relation of the form: $\log r_e = 1.5 \log \sigma - 0.8 \log I_e$. It is not yet clear why the virial fundamental plane is not the same as the observed fundamental plane. This observed discrepancy between the virial and observed fundamental plane is known as the tilt of the fundamental plane. Systematic variations in the mass-to-light ratio or non-homology effects that lead to a systematic change of the surface brightness profile with increasing luminosity might explain the tilt.

2.5 Elliptical galaxies and the MOND Fundamental Plane relation

In MOND high surface brightness elliptical galaxies are not expected to show, within the optical radius, a large discrepancy between the mass- and light distribution. The high surface brightness of the elliptical galaxies implies that the internal accelerations are high compared to a_0. MOND is thus in the Newtonian regime where mass estimates from the luminous matter should explain the dynamical mass.

Sanders (2000) used isotropic and isothermal spheres to model elliptical galaxies in MOND. But in the velocity dispersion-effective radius relation, the MOND models showed a lower surface density then observed. The internal accelerations of the galaxies were underestimated in these simple models. In order to explain the observed velocity dispersion, effective radius and surface density of elliptical galaxies, they must deviate from isothermal and isotropic spheres. The velocity distribution has to increase outwards and stellar orbits became more radial in the outer regions. Systems formed from dissipationless collapse do have an inner region which is isotropic while their outer region has a radial velocity distribution (van Albada, 1982). Deviation from a constant velocity dispersion is observed by Franx (1988): the line of sight velocity dispersion does decrease with radius with a power law: $\sigma \propto r^{-\epsilon}$, whith $\epsilon = 0.06$ for a typical elliptical galaxy.

In MOND these deviations from isothermal and isotropic spheres can be incorporated by a polytropic equation of state with a large polytropic index n:

$$\sigma_r^2 = A_{n\sigma} \rho^{1/n}, \tag{13}$$

9

with $A_{n\sigma}$ a constant depending on the model and σ_r the velocity dispersion in the radial direction. In contrast to the Newtonian case where only polytropic spheres with a polytropic index smaller than 5 are finite in extent and mass, MOND produces always finite polytropic spheres in extent and mass. MOND polytropic spheres with $n > 5$ have an inner Newtonian region where the outer boundary conditions are established by the MOND regime. For $n > 10$ the outer region of the sphere is always in the MOND regime. The polytropic index $n > 5$ is thus a free parameter of the models.

Together with the radial anisotropy parameter $\beta(r)$:

$$\beta(r) = \frac{(r/r_a)^2}{1 + (r/r_a)^2} \tag{14}$$

where r_a is the anisotropy radius, MOND has sufficient degrees of freedom to explain the observed velocity dispersion - effective radius relation of elliptical galaxies.

For high order anisotropic polytropic spheres Sanders (2000) showed that the mass-velocity dispersion relation has the form:

$$\sigma_o^4 = q(n, \eta) \, GMa_0 \tag{15}$$

where σ_o is the central line-of-sight velocity and $q(n, \eta)$ is the ratio between σ_o^4 and GMa_0. For pure isothermal spheres $q = 1/16$, for high order polytropic spheres q can be approximated by a power-law depending on the mean surface density Σ in units of the MOND critical surface density $\Sigma_m = a_0/G$:

$$q = k \left(\Sigma/\Sigma_m\right)^\kappa. \tag{16}$$

To reproduce the observed properties of elliptical galaxies, $\eta = r_a a_0/\sigma_r^2$ the anisotropy radius in terms of the characteristic MOND length, is restricted to be larger than 0.2, otherwise the radial orbits are not stable, and n is restricted to $12 < n < 16$ in order to reproduce the observed decline in the line-of-sight velocity dispersion.

Using an ensemble of anisotropic polytropes with the anisotropy radius and polytropic index in the range as defined in the previous paragraph, Sanders' (2000) best fit result is

$$M/\left(10^{11} M_\odot\right) = 3 \times 10^{-5} \sigma_d^{1.76} r_e^{0.98} \tag{17}$$

with σ_d the velocity dispersion within a finite aperture with radius r_d. The velocity dispersion is in kms^{-1} and the effective radius in units of kpc. This MOND fundamental plane does resemble the Newtonian virial fundamental plane, where the exponents for σ and r are 2 and 1 respectively.

3   Modelling of stellar kinematics

The SAURON project is a program to determine the kinematics and stellar populations of 72 cluster and field E, S0 and Sa galaxies in our near vicinity.
For this research project, data from the Cappellari et al. (2006) paper is used to test the fundamental plane relation for the 25 E/S0 galaxies in the sample. The measured parameters are in Table 1 of Cappellari et al. (2006). Since not all galaxies in the sample are observed out to r_e, the velocity dispersion has to be corrected to create a uniform sample. The same correction as Cappellari et al. (2006) applied to create a uniform sample is used:

$$\sigma_e = \sigma_R \left(\frac{R}{r_e} \right)^{0.066 \pm 0.035} \tag{18}$$

where σ_R is the velocity dispersion within radius R and σ_e is the velocity dispersion within the effective radius, r_e. The central line of sight velocity, σ_o, which was used in the models of Sanders (2000) is replaced by the luminosity-weighted second moment of the line of sight velocity distribution, σ_e, used by Cappellari et al. (2006).
Figure 1 shows the best fitting fundamental plane relation for a set of 360 polytropic models. Instead of the central line-of-sight velocity distribution used by Sanders (2000) the luminosity weighted second moment of the line-of-sight velocity is used to create the fundemantel plane. In the top panel the σ_e-mass relation is given. When the effective radius is added to the plane the scatter is significantly reduced. For the Cappellari et al. data, $\gamma = 0.58$ and the slope of the fundamental plane with the least scatter is 1.85. This results in a slightly different form of Eq. (17):
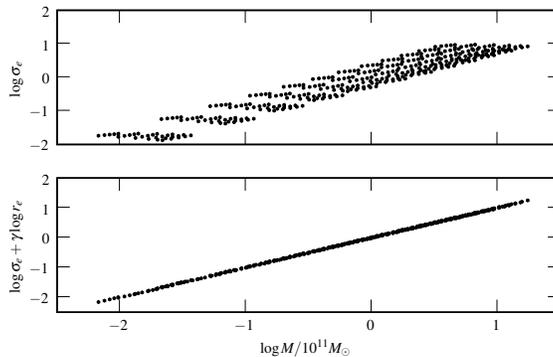

Figure 1: The best fitting fundamental plane relation for a set of 360 polytropic models. In the top panel the mass-velocity dispersion related is plotted, while in the bottom panel the effective radius is added. The parameter γ is chosen such that the scatter is minimised. The resulting slope is 1.85 with $\gamma = 0.58$. The scatter in the bottom panel is significant less compared to the scatter in the top panel.

11
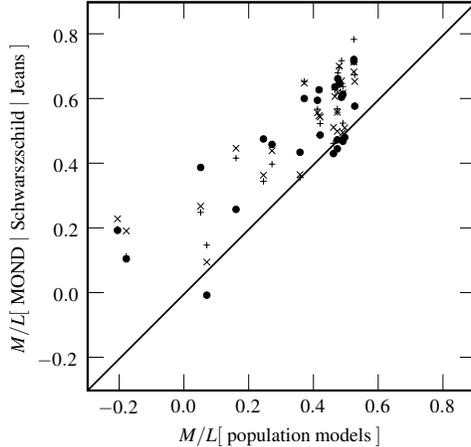
Figure 2: Mass-to-light ratios for population models plotted against calculated mass-to-light ratios for the galaxies observed in the Cappellari et al. (2006) paper. The MOND derived mass-to-light ratios are given by filled circles. The crosses and plus sign symbols are the two-integral Jeans model and the Schwarzschild three-integral models, respectively. Overall the MOND mass-to-light ratios have the smallest deviation from the one-to-one relation line plotted in the figure.

$$M/\left(10^{11} M_\odot\right) = 2 \times 10^{-5} \sigma_e^{1.85} r_e^{1.07} \tag{19}$$

where σ_e is in units of km/s and r_e in kpc.

3.1 Comparing mass-to-light ratios

With the data from Cappellari et al. (2006) the stellar mass estimates from population models can be compared to masses derived from the fundamental plane relation, Eq. (19). The populations models used by Cappellari et al. (2006) are created by Vazdekis et al. (1996); single burst stellar population models.

In Figure 2 the stellar population models mass-to-light ratios are compared to mass-to-light ratios with either a MOND polytropic model or the two mass estimates from Cappellari et al. (2006). The MOND mass-to-light ratios compared to the stellar population models show a slight overestimation of the mass-to-light ratio compared to the one-to-one correlation with the stellar population models. For the Schwarzschild and Jeans estimates of the mass-to-light ratios there is still a correlation between the models and the calculated mass-to-light ratios, but with a slope deviating more from the one-to-one correlation compared to the MOND case. The mean ratio between the mass estimates from Cappellari et al. (2006) and the MOND fundamental plane is only 1.06, which shows that within an effective radius MOND mass estimates do not deviate much from the Schwarzschild and Jeans models.

12

The mean M/L ratio as a function of mass for the sample of galaxies estimated from the MOND fundamental plane is 3.3, with a scatter of 30 percent. These numbers are comparable for the Schwarzschild model mass-to-light estimate from Cappellari et al. This relation is shown in Figure 3. The dependency of the M/L ratio on mass is weak, with $M/L \propto M^{0.24}$ for the MOND method and $M/L \propto M^{0.27}$ for the data from Cappellari et al.
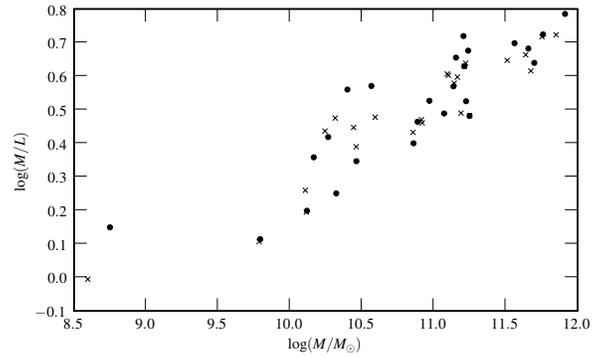

Figure 3: The mass-to-light ratio of the galaxies from Cappellari et al. (2006) as function of mass. The crosses are the Schwarzschild model generated mass-to-light ratios and masses while the filled circles are mass-to-light ratios and masses derived from the MOND fundamental plane relation.

13

4 Lensing

In general relativity light does not travel in a straight line but follows the geodesic of the metric. The presence of a gravitational potential curves the metric and a passing light ray is bent. In the weak field limit this bending of light can be quantified by using the deflection angle α:

$$\alpha \approx \frac{2}{c^2} \int\limits_{-\infty}^{\infty} dl\, g_\perp(r),$$
(20)

where l is the distance along the line of sight, $r = \sqrt{l^2 + b^2}$ and $g_\perp = g(r)b/r$ is the gravitational acceleration transversel to the direction of the motion of the photon, b is the impact parameter.

If Newtonian physics and spherical symmetry is assumed, the gravitational field is given by

$$g_N = \frac{GM}{r^2},$$
(21)

where M is the enclosed (point) mass. With MOND this gravitational field is changed into

$$g_M = \begin{cases} \sqrt{a_0 g_N} & g_N < a_0 \\ g_N & \text{otherwise.} \end{cases}$$
(22)

Integrating the deflection angle (Eq. 20) for both general relativity and MOND, the angle in a sphericaly symmetric system with a point-mass distribution is:

$$\alpha = \begin{cases} \frac{4GM}{c^2 b} & \text{general relativity} \\ \frac{4GM}{c^2 b}\sqrt{1 - \left(\frac{b}{r_0}\right)^2} + \frac{4}{c^2}\sqrt{GMa_0}\sin^{-1}\left(\frac{b}{r_0}\right) & b < r_0 \\ \frac{2\pi}{c^2}\sqrt{GMa_0} & b > r_0, \end{cases}$$
(23)

where $r_0 = \sqrt{GM/a_0}$. The first equation of the three is valid for general relativity and the final two equations are valid for MOND.

In Figure 4 the deflection angle α is plotted as a function of the impact parameter b in units of kpc. The mass of the point-mass as source of the lens is assumed to be $10^{11} M_\odot$, a median mass for lenses observed by the Sloan Lens ACS Survey. Up to 10 kpc the deflecting angle in MOND does not deviate from the deflection angle in general relativity. This result allows the use of the well understood general relativity theory for gravitational lensing for mass estimates at distances up to 10 kpc from the centre of the lens.

Figure 5 shows the light-ray path from an emitting source with an offset x from the line observer-lens. The light-ray is deflected by the massive gravitational lens in the middle of the figure. Since all angles involved are small the distance x is given by:

$$x = D_s\theta - D_{sl}\alpha,$$
(24)
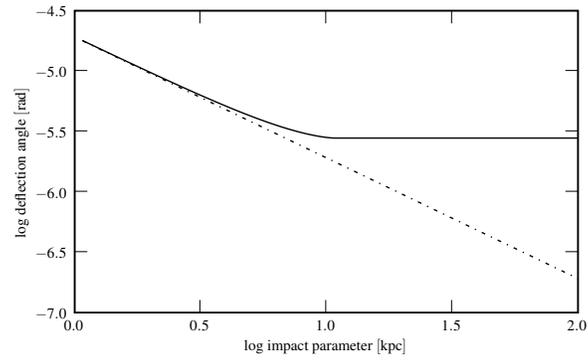
Figure 4: The deflection angle of a lens with a point-mass of $10^{11} M_{\odot}$ as a function of impact parameter. The deviation from general relativity only occurs after $10\,kpc$ from the centre of the lens.
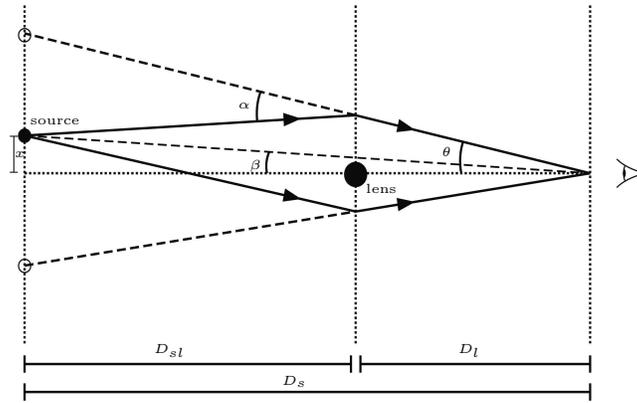
Figure 5: Schematic drawing of a gravitational lensing system. The angle of deflection is α.

with α the deflection angle. The minimum distance from the light ray to the lens is $b = \theta D_l$, the impact parameter from Eq. 23. For a system where the lens, source and observer are on the same line, $x = 0$. Substituting α from Eq. (20) into Eq. (24) the mass of the lens within a surface with radius $b = \theta D_l$ is:

$$M = \frac{\theta^2 c^2}{4G} \frac{D_s D_l}{D_{sl}}.$$ (25)

In this equation θ is the angular radius of the lensed image. When the distance to the lens, D_l, the source, D_s and the angle of seperation between different sources 2θ are known, the mass of the lens can be obtained from Eq. (25). Without depending on the luminous matter of the lens.

4.1 The 'more' fundamental plane

Bolton et al. (2007) applied the lensing mass determination to the fundamental plane relation in order to remove the mass-to-light ratio dependency of the fundamental plane. They selected 36 early type lenses from the Sloan Lens ACS Survey with a redshift range of $z_{\text{lens}} \sim 0.1 - 0.4$ and an absolute magnitude in the V band in the range $M_V = -20.8$ to -24.0.
The lensing data was used to remove the surface brightness I of the fundamental plane and replace it by the surface mass density Σ_{e2} within $r_e/2$, half the effective radius. By doing so the fundamental plane relation has the form

$$\log r_e = a \log \sigma_{e2} + b \log \Sigma_{e2} + d,$$ (26)

with σ_{e2} the velocity dispersion within half an effective radius.
Bolton et al. (2007) found as coefficients for the mass fundamental plane: $a = 1.77 \pm 0.14$, $b = -1.16 \pm 0.09$ and $d = 7.8 \pm 1.0$, using an isothermal model for the mass determination of the lensing data. If a model is used where the mass is assumed to trace the light the coefficients are $a = 1.86 \pm 0.17$, $b = -0.93$ and $d = 5.4 \pm 0.9$.

4.2 MOND and the 'more' fundamental plane

In the 'more' fundamental plane observed by Bolton et al. (2007) the observables are the effective radius, velocity dispersion within half an effective radius and the surface mass density within the same radius. Figure 6 shows the MOND fundamental plane relation for a set of 360 anisotropic polytropic models. The same method as in Sanders (2000) is used, with the surface brightness replaced by the surface mass density. The plane where the scatter is minimised using the best fit value for γ is:

$$\log r_e = 1.99 \log \sigma_{e2} - 1.06 \log \Sigma_{e2} + 6.14$$ (27)

with a comparable scatter as in the 'original' MOND fundamental plane relation by Sanders (2000). This MOND fundamental plane agrees with the 'more'
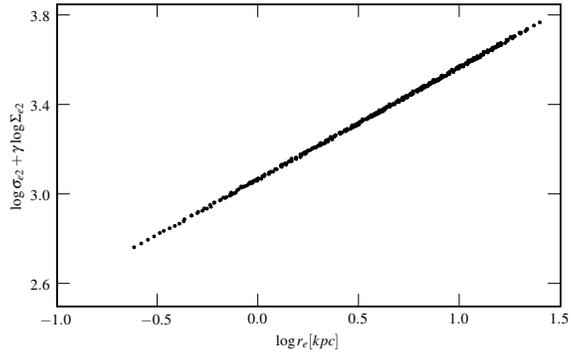
Figure 6: The best fitting fundamental plane relation for a set of 360 polytropic models with the same observables as the 'more' fundamental plane. The slope is 1.99 with $\gamma = 0.53$ to minimise the scatter.
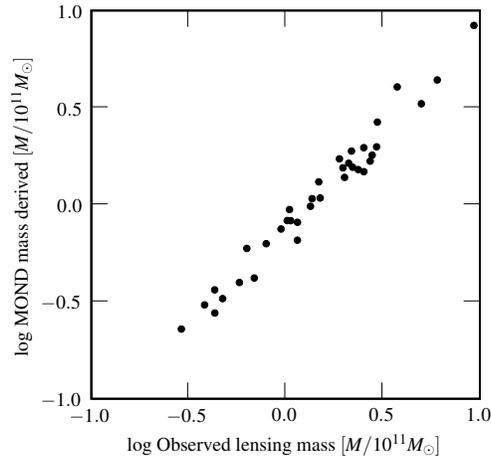
Figure 7: The MOND mass derived from the fundamental plane relation versus the observed lensing mass.

17

fundamental plane, Eq. 26, for both the isothermal models and light-trace mass model. With the fundamental plane relation as given by Eq. (27) the mass of the lens can be obtained by rewriting the surface mass density to a mass within half an effective radius.

Figure 7 shows masses derived from the MOND fundamental plane relation and the masses observed from the lensing data by Bolton et al. (2007). The lensing mass within the Einstein radius is extrapolated to a mass estimate within half the effective radius from the fundamental plane relation. Since the median ratio between the effective and Einstein radius is 0.55, the interpolation does not change the sample much. In the figure the correlation between the observed mass and the mass derived from the MOND fundamental plane relation is striking. All the observed mass is explained by the MONDian fundamental plane without the need for any dark matter.

4.3 Mass-to-light ratios

Bell et al. (2003) used a sample from the SDSS and 2MASS galaxy catalogues from which they calculated stellar mass and galaxy luminosity functions for the local universe. From this sample they obtained relations between various colours and stellar mass-to-light ratios. The mass-to-light ratios in the r band and the $(r - i)$ colour are related:

$$\log_{10}\left(\frac{M}{L_r}\right) = -0.022 + 1.431\,(r - i) - 0.15\,. \qquad (28)$$

The last term in Eq. 28 is a correction for the underestimation of the number of low mass objects formed because of the Kroupa or Kennecut initial mass function used in the stellar population models.

In Figure 8 the theoretical mass-to-light ratio as a function of colour is compared to both the MOND fundamental plane and the relation found by Bolton et al. (2007). In the top panel the MOND fundamental plane relation is used to determine the mass, the luminosity is obtained from the Sloan Digital Sky Survey in the r passband. In the bottom panel the 'more' fundamental plane from Bolton et al. (2007) is used instead. Almost all MOND data points do fall in the uncertainty range for the theoretical model. The 'more' fundamental plane observed mass-to-light ratios are on average slightly higher than the predicted mass-to-light ratios from Bell et al. (2003).

The magnitudes are corrected for redshit and evolution from the models of Poggianti (1997) where the models of elliptical galaxies with an e-folding time of 1 Gyr are used. For the distance determination from the redshift of the lenses the concordance model is used, with an Hubble constant of 73 km/s/Mpc.

4.4 Conclusion

The fundamental plane relation does also exists in MOND context. Sanders (2000) showed that the observed properties of elliptical galaxies can be explained by using anisotropic high order polytropic spheres.

18
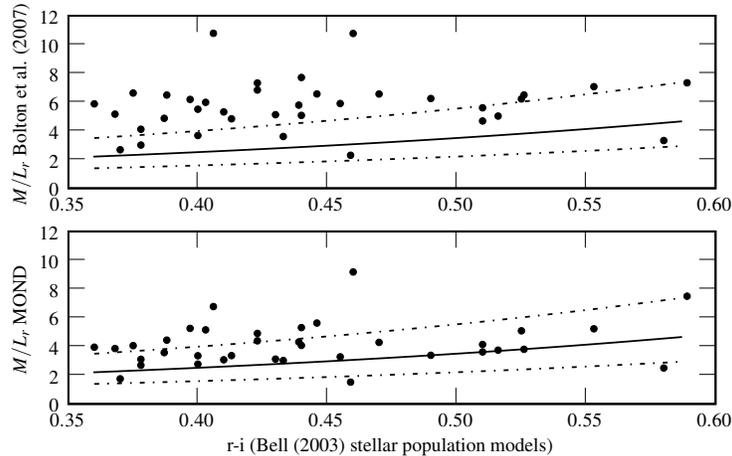
Figure 8: In the top panel the theoretical mass-to-light ratio as a function of $(r - i)$ colour (line), Eq. (28), is compared to the MOND derived mass-to-light ratio from the fundamental plane relation (filled circles). In the bottom panel the same theoretical model (line) is compared to the lensing masses from Bolton et al. (2007) (filled circles). The dash-dotted lines are the 0.2 dex spread in the theoretical mass-to-light ratio according to Bell et al. (2003), which give an indication of the errors in the theoretical models.

The same model from Sanders (2000) is adapted for the observables of the 'more' fundamental plane and the 'more' fundamental plane constructed by Bolton et al. (2007) is compared to the MOND fundamental plane for the lensing data set. Using the mass measurements of the lenses, the mass estimates of the MOND fundamental plane explain the observed matter.

Besides explaining the matter observed by the lensing measurements, both MOND and the 'more fundamental plane' agree well with the stellar population model mass-to-light ratios. The MOND mass-to-light ratios are on average lower than the mass-to-light ratios from Bolton et al. (2007). This is because the MOND mass estimates are the total baryonic mass of the system, estimated from the velocity dispersion and the effective radius, while the mass estimates from the lensing models due assume some pseudo dark matter since a MOND relativist theory would provide some extra deflection along the line of sight.

19

5 Hot Gas

5.1 Mass from hot gas

The mass of a galaxy consists of the mass of the gas included in the galaxy and the mass of the stars. There might be some dark matter content to explain the dynamical mass by the luminous matter distribution.

For a spherically symmetric gas density distribution $\rho(r)$, the gas mass profile is given by a volume integral over the gas density distribution:

$$M_{\text{gas}}(r) = 4\pi \int_0^r \rho(r')r'^2 dr', \tag{29}$$

where $M_{\text{gas}}(r)$ is the total gas mass contained within a radius r.

Galaxies not only contain gas, but also other matter (stars, planets, etc.). To be able to derive the total dynamical mass of a galaxy from the hot gas observed, some assumptions need to be made. One of those is hydrostatic equilibrium: the outward force of pressure dP/dr is equal to the inward Newtonian force of gravity g_N times the gas density ρ

$$\frac{dP}{dr} = -g_N\rho. \tag{30}$$

Assuming an ideal gas, the gas pressure gradient can be rewritten in gradients in the temperature and density. Assuming spherical symmetry the gravitational acceleration is related to the total dynamical mass within a radius r, resulting in the dynamical mass profile:

$$M_N(<r) = \frac{kT(r)r}{\mu m_H G} \left(\frac{d\log_e \rho}{d\log_e r} + \frac{d\log_e T}{d\log_e r} \right)_r, \tag{31}$$

where k is the Boltzmann constant, $T(r)$ the temperature profile, μ the average molecular ratio, m_H the mass of the hydrogen atom, ρ the gas density and $M_N(<r)$ the mass within a sphere with radius r.

In the MOND regime the Newtonian gravitational acceleration is replaced by the true gravitational acceleration, g:

$$\frac{dP}{dr} = -g\rho \tag{32}$$

If Eq. (3) with the interpolation function $\mu(x) = x(1 + x^2)^{-1/2}$ is used, the MOND dynamical mass as a function of the Newtonian dynamical mass is obtained:

$$M_{\text{MOND}}(<r) = \frac{M_N(<r)}{\sqrt{1 + (a_0/a)^2}}, \tag{33}$$

where $a = \frac{1}{\rho}\frac{dP}{dr}$ is the acceleration. The MOND mass reduces to the Newtonian dynamical mass in the limit of large accelerations, as is expected from the interpolation function. Summing both the gas mass (Eq. 29) and the dynamical mass (Eq. 33) estimates gives the total mass profile of a galaxy.

5.2 X-ray observations

With the X-ray satellites Chandra and XMM-Newton it is possible to study in detail the structure and content of hot X-ray emitting gas in the cores of clusters of galaxies. Assuming hydrostatic equilibrium the dynamical mass of such a system can be obtained. To determine the individual properties of the group members is a danting task. Other galaxies in the same group influence the overal properties and make it difficult to constrain the luminous matter, gas content and dynamical mass to one object. Another difficulty in the case of dark matter is that the cluster has its own dark matter halo.

Observing isolated elliptical galaxies does solve most of these problems. But isolated elliptical galaxies are not common in the universe, most of them are located in the center of clusters and super clusters of galaxies.

Humphrey et al. (2006), O'Sullivan et al. (2007) and O'Sullivan and Ponman (2004) studied a total of 11 elliptical galaxies of which 7 are isolated. The galaxies observed by O'Sullivan et al. (2007) are NGC 7796, NGC 57 and IC 1531. They are relatively isolated and are in low density environments. IC 1531 has a compact core and the authors assume gas has been removed from it due to active galactic nucleus heating. NGC 57 was observed by XMM-Newton, NGC 7796 by Chandra and IC 1531 by both X-ray satellites. O'Sullivan and Ponman (2004) observed NGC 4555 with Chandra. Humphrey et al. (2006) observed 7 elliptical galaxies with Chandra, of which NGC 720, NGC 4125 and NGC 6482 are used in this work.

For those 7 isolated galaxies the total mass, mass-to-light ratio and gas mass are calculated from the X-ray gas density and temperature profiles. Using hydrostatic equilibrium (Eq. 31) the dynamical mass in Newtonian dynamics is calculated.

Galaxy	M_N/L_B	M_m/L_B	M/L measurement [kpc]
NGC 57	$48.4^{+4.7}_{-10.3}$	$29.2^{+4.7}_{-9.7}$	55.0
NGC 720	$213.6^{+77.6}_{-97.1}$	$7.1^{+6.1}_{-5.0}$	480.0
NGC 4125	$132.5^{+17.2}_{-49.1}$	$4.3^{+1.2}_{-2.6}$	470.0
NGC 4555	$56.8^{+34.2}_{-35.8}$	$48.1^{+36.6}_{-37.4}$	50.0
NGC 4555	$42.7^{+14.6}_{-21.2}$	$17.9^{+12.3}_{-13.0}$	80.6 $(5r_e)$
NGC 6482	$64.8^{+40.1}_{-15.6}$	$2.1^{+3.5}_{-0.9}$	500.0
NGC 7796	$10.6^{+2.5}_{-2.3}$	$7.9^{+2.7}_{-2.4}$	28.4

Table 1: The mass-to-light ratios for the 6 galaxies. In the last column the distance from the center of the galaxy to the location of the M/L measurement is given. The Newtonian M/L values are those calculated by the authors. For NGC 57 and NGC 7796 the M/L ratio is calculated around $5r_e$, for NGC4555 the ratios are calculated both at $5r_e$ and at 50 kpc, while for the galaxies from Humphrey et al. (2006) the mass profile extends to several hundreds of kpc.

In order to obtain the MOND dynamical mass estimates for the galaxies the Newtonian masses are multiplied by the MOND correction (Eq. 33). Since MOND is only different from Newtonian Dynamics in the low acceleration regime, away from the centre of the galaxy the mass estimates at larger effective radius are more favourable in explaining the observed mass profile using MOND. For mass estimates in the inner part of a galaxy, there is no real difference expected between MOND and purely Newtonian dynamics.

In Table 1 the Newtonian and MOND M/L estimates are given. For the galaxies observed by Humphrey et al. (2006) the M/L ratios are lower by orders of magnitude, while for the galaxies observed by O'Sullivan et al. (2007) and O'Sullivan and Ponman (2004) the need for dark matter is reduced, but not as significantly as for the other three galaxies. The mass of NGC 4555 is determined twice at different radius. The reduction in mass-to-light ratio in the Newtonian case is most likely due to different density and temperature profiles. Since the luminosity is determined in the inner regions the mass-to-light ratio is expted to be either the same or higher compared to measurements more inwards. Within the error margins the measurements at both distances agree.

5.3 Hydrostatic equilibrium

In order to derive the mass from the observed X-ray temperature and density, the assumption of hydrostatic equilibrium must be valid. Diehl and Statler (2007) used a sample of 54 elliptical galaxies observed by Chandra and compared their X-ray temperature and density with the optical data from 2MASS, Digitized Sky Survey and Hyperleda. They isolated the X-ray gas emission from the stellar emission by identifying point-sources and removing them (including the wings induced from the point spread function). Low mass X-ray binaries were removed using their known spectral properties as a template for the unresolved ones.

With the X-ray emission separated from the stellar emission, the morphology can be compared. Diehl and Statler (2007) found that in general the X-ray gas does not follow the potential derived from the stellar mass. Within one or two optical effictive radii the potential is assumed to be dominated by the stellar mass (Lintott et al., 2006), which indicates that gas is not following the stellar potential, either because of another, dark, potential or the gas is not in hydrostatic equilibrium.

Diehl and Statler (2007) found no correlation between the optical and X-ray ellipticity and no evidence for transfer of angular momentum from stellar mass loss to the gas halo. In a dark matter dominated Universe this puts tight constraints on the shape and distribution of the dark matter halo. To keep the gas in hydrostatic equilibrium the dark matter content of the galaxy need to extent into the interior, with 10 times as much dark matter as stellar mater in the stellar half-mass radius or the dark matter halo needs to be cigar or sausage shaped.

If hydrostatic equilibrium is not true for the gas content, the mass estimates from the gas content of galaxies are overestimated. For a normal galaxy with

a region that was overpressured by a factor of a few, this would result in a overestimate of the mass by the same factor.

5.4   Conclusions

MOND explains the matter observed in some of the elliptical galaxies without the need for dark matter. The farther away from the centre, the better MOND describes the dynamical mass estimates compared to the stellar mass. With the results from Diehl and Statler (2007) the high mass-to-light ratios for NGC 4555 and NGC 57 can be explained. The assumption of hydrostatic equilibrium is not valid, which overestimates the mass measurements from the X-ray data. For NGC 4555 the difference between $5r_e$ and 50 kpc from the centre of the galaxy is quite obvious. The mass-to-light ratio drops significant in the MOND case. Even in the Newtonian case the mass-to-light ratio farther out of the galaxy is lower, but this is more likely due to different density and temperature profiles. The errors on the mass-to-light ratios at both distances do overlap.

6   Overall conclusions

In this work different mass estimates are used to determine the mass of a galaxy:

- The MOND fundamental plane relation for both a set of gravitational lenses observed by the Sloan Lens ACS Survey.

- Galaxies observed with SAURON.

- Hot X-ray gas from Chandra and XMM-Newton in isolated elliptical galaxies.

For all these mass estimates the MOND mass agrees with theoretical mass estimates derived from the luminous matter without requiring additional (dark) matter. For the lensing mass estimates both the MOND fundamental plane and the 'more' fundamental plane require little or no dark matter, which is expected in the energetic inner parts of the galaxies.
For mass estimates in the outskirts of the galaxies, the differences between MOND and Newtonian dynamics is large. Since Newtonian dynamics needs a lot of dark matter to sustain the hot gas determined mass-to-light ratios of a few hundred are not uncommon. For MOND the mass-to-light ratios drop to values similar to stellar population mass-to-light ratios. The assumption of hydrostatic equilibrium necessary to deduce the mass from the X-ray data seems to be an oversimplification for real elliptical galaxies. The dynamical masses of the galaxies which are not in equilibrium might be a factor of two smaller than deduced from the X-ray data.

6.1   Future work

Extensive work in determining the mass-to-light ratio in spiral galaxies has been done. In the case of isolated elliptical galaxies there are still more galaxies to observe and analyse. With MOND and with a dark matter halo, to try to distinguish between the scenarios.
With the lensing mass estimates available, there is an independent measurement of the mass of the galaxy. The lensing data can put constraints on the shape of a dark matter halo, or the shape of the interpolating function from Newtonian dynamics to the region where MOND is dominating.

Acknowledgements

References

Begeman, K. G., Broeils, A. H., and Sanders, R. H. (1991). Extended rotation curves of spiral galaxies - Dark haloes and modified dynamics. *MNRAS*, 249:523–537.

Bell, E. F., McIntosh, D. H., Katz, N., and Weinberg, M. D. (2003). The Optical and Near-Infrared Properties of Galaxies. I. Luminosity and Stellar Mass Functions. *ApJS*, 149:289–312.

Bernardi, M., Sheth, R. K., Annis, J., Burles, S., Eisenstein, D. J., Finkbeiner, D. P., Hogg, D. W., Lupton, R. H., Schlegel, D. J., SubbaRao, M., Bahcall, N. A., Blakeslee, J. P., Brinkmann, J., Castander, F. J., Connolly, A. J., Csabai, I., Doi, M., Fukugita, M., Frieman, J., Heckman, T., Hennessy, G. S., Ivezić, Ž., Knapp, G. R., Lamb, D. Q., McKay, T., Munn, J. A., Nichol, R., Okamura, S., Schneider, D. P., Thakar, A. R., and York, D. G. (2003). Early-Type Galaxies in the Sloan Digital Sky Survey. III. The Fundamental Plane. *AJ*, 125:1866–1881.

Bolton, A. S., Burles, S., Treu, T., Koopmans, L. V. E., and Moustakas, L. A. (2007). A More Fundamental Plane. *ArXiv Astrophysics e-prints*.

Canizares, C. R. (1982). Manifestations of a cosmological density of compact objects in quasar light. *ApJ*, 263:508–517.

Cappellari, M., Bacon, R., Bureau, M., Damen, M. C., Davies, R. L., de Zeeuw, P. T., Emsellem, E., Falcón-Barroso, J., Krajnović, D., Kuntschner, H., Mc-Dermid, R. M., Peletier, R. F., Sarzi, M., van den Bosch, R. C. E., and van de Ven, G. (2006). The SAURON project - IV. The mass-to-light ratio, the virial mass estimator and the Fundamental Plane of elliptical and lenticular galaxies. *MNRAS*, 366:1126–1150.

Carr, B. J., Bond, J. R., and Arnett, W. D. (1984). Cosmological consequences of Population III stars. *ApJ*, 277:445–469.

Clausius, R. (1870). *De la fonction potentielle DU Potentiel*. Paris : Gauthier-Villars, 1870; XIV, 141 p. ; in 8.; DCCC.4.398.

Cooley, J. (2006). Status and Perspectives of Dark Matter Searches. *ArXiv Astrophysics e-prints*.

Diehl, S. and Statler, T. S. (2007). The Hot Interstellar Medium of Normal Elliptical Galaxies. I. A Chandra Gas Gallery and Comparison of X-Ray and Optical Morphology. *ApJ*, 668:150–167.

Djorgovski, S. and Davis, M. (1987). Fundamental properties of elliptical galaxies. *ApJ*, 313:59–68.

Dressler, A., Lynden-Bell, D., Burstein, D., Davies, R. L., Faber, S. M., Terlevich, R., and Wegner, G. (1987). Spectroscopy and photometry of elliptical galaxies. I - A new distance estimator. *ApJ*, 313:42–58.

Efstathiou, G. and Silk, J. (1983). The formation of galaxies. *Fundamentals of Cosmic Physics*, 9:1–138.

Franx, M. (1988). *Structure and kinematics of elliptical galaxies.* Leiden: Rijk-suniversiteit, 1988.

Humphrey, P. J., Buote, D. A., Gastaldello, F., Zappacosta, L., Bullock, J. S., Brighenti, F., and Mathews, W. G. (2006). A Chandra View of Dark Matter in Early-Type Galaxies. *ArXiv Astrophysics e-prints.*

Lintott, C. J., Ferreras, I., and Lahav, O. (2006). Massive Elliptical Galaxies: From Cores to Halos. *ApJ*, 648:826–834.

Milgrom, M. (1983). A modification of the Newtonian dynamics as a possible alternative to the hidden mass hypothesis. *ApJ*, 270:365–370.

O'Sullivan, E. and Ponman, T. J. (2004). The isolated elliptical NGC 4555 observed with Chandra. *MNRAS*, 354:935–944.

O'Sullivan, E., Sanderson, A. J. R., and Ponman, T. J. (2007). The dark haloes of early-type galaxies in low-density environments: XMM-Newton and Chandra observations of NGC 57, 7796 and IC 1531. *MNRAS*, pages 746–+.

Poggianti, B. M. (1997). K and evolutionary corrections from UV to IR. *A&AS*, 122:399–407.

Rogstad, D. H. and Shostak, G. S. (1972). Gross Properties of Five Scd Galaxies as Determined from 21-CENTIMETER Observations. *ApJ*, 176:315–+.

Ryden, B. (2003). *Introduction to cosmology.* Introduction to cosmology / Barbara Ryden. San Francisco, CA, USA: Addison Wesley, ISBN 0-8053-8912-1, 2003, IX + 244 pp.

Salpeter, E. E. (1955). The Luminosity Function and Stellar Evolution. *ApJ*, 121:161–+.

Sanders, R. H. (2000). The fundamental plane of elliptical galaxies with modified Newtonian dynamics. *MNRAS*, 313:767–774.

Sanders, R. H. and McGaugh, S. S. (2002). Modified newtonian dynamics as an alternative to dark matter. *Annu. Rev. Astron. Astrophysics.*

Spergel, D. N. (1988). Motion of the Earth and the detection of weakly interacting massive particles. *Phys. Rev. D*, 37:1353–1355.

Tisserand, P., Le Guillou, L., Afonso, C., Albert, J. N., Andersen, J., Ansari, R., Aubourg, É., Bareyre, P., Beaulieu, J. P., Charlot, X., Coutures, C., Ferlet, R., Fouqué, P., Glicenstein, J. F., Goldman, B., Gould, A., Graff, D., Gros, M., Haissinski, J., Hamadache, C., de Kat, J., Lasserre, T., Lesquoy, É., Loup, C., Magneville, C., Marquette, J. B., Maurice, É., Maury, A., Milsztajn, A., Moniez, M., Palanque-Delabrouille, N., Perdereau, O., Rahal, Y. R., Rich, J., Spiro, M., Vidal-Madjar, A., Vigroux, L., Zylberajch, S., and The EROS-2 Collaboration (2007). Limits on the Macho content of the Galactic Halo from the EROS-2 Survey of the Magellanic Clouds. *A&A*, 469:387–404.

van Albada, T. S. (1982). Dissipationless galaxy formation and the R to the 1/4-power law. *MNRAS*, 201:939–955.

Vazdekis, A., Casuso, E., Peletier, R. F., and Beckman, J. E. (1996). A New Chemo-evolutionary Population Synthesis Model for Early-Type Galaxies. I. Theoretical Basis. *ApJS*, 106:307–+.

Weinberg, S. (1972). *Gravitation and Cosmology: Principles and Applications of the General Theory of Relativity.* Gravitation and Cosmology: Principles and Applications of the General Theory of Relativity, by Steven Weinberg, pp. 688. ISBN 0-471-92567-5. Wiley-VCH , July 1972.

Zwicky, F. (1937). On the Masses of Nebulae and of Clusters of Nebulae. *ApJ*, 86:217–+.